Journal of Applied Physics, vo.63, No. 12

Analysis of lattice strains measured under nonhydrostatic pressure

Anil K. Singh and C. Balasingh
materials Science D, National Aerospace *Laboratories, Bangalore* 560 017, Indio
division
Ho-kwang Mao, Russell J. Hemley, and Jinfu Shu
G,eophv.cual Lcrborarori and Center for High Pressure Resrarch, Carnegie Institution of Washington, 5251 Broad Branch Road .V. W., Washin,gto+t D.C. 2001.5.130.5

(Received I 1 November 1997; accepted for publication 27 February 1998)

The equations for the lattice strains produced by nonhydrostatic compression are presented for all seven crystal systems in a form convenient for analyzing x-ray diffraction data obtained by newly developed methods. These equations have been used to analyze the data on cubic (hcc a-Fe) and hexagonal (hcp E-Fe) systems. The analysis gives information on the strain produced by the hydrostatic stress component. A new method of estimating the uniaxial stress component from diffraction data is presented. Most importantly, the present analysis provides a general method of determining single crystal elastic constants to ultrahigh pressures. © 1998 *Phti:sics. (S0021-8979(98)0311 I -9]*

I. INTRODUCTION

The improved design of the diamond anvil cell has made it possible to reach *pressures in the range* of several hundred gigapascals, [1,2] and the use of synchrotron radiation as the source of incident x rays allows diffraction patterns to be recorded from materials compressed under such conditions.[3–7] Because of the finite shear strength of the specimen material, the stress state of the compressed sample is in general not hydrostatic.[8] Early experiments[9,10] on materials subjected to nonhydrostatic stress states (NSS) led to the development of mathematical formulations of NSS and its effect on the lattice strains.[11–13] Equations for the lattice strains under NSS for cubic,[14,15] hexagonal,[16] and trigonal[17] systems were *developed* that are valid for a general diffraction geometry. Equations for all crystal systems have been derived recently.[18] The full utilization of the equations in the interpretation of the lattice strain data and extraction of the sample properties became possible through the introduction of two new diffraction geometries;[19–21] these permit the measurement of d spacings as a function of the angle, ψ, between the diffraction vector and the load direction. In this article we present the lattice-strain equations for all the crystal systems in a form convenient for the interpretation of diffraction data. We then show that the strain produced by the hydrostatic stress component can be separated out from the lattice strains measured under NSS. A new method of estimating the uniaxial stress component is suggested, and the possibility of estimating the single crystal elastic constants from the powder diffraction data obtained under nonhydrostatic compression is demonstrated.

II. EQUATIONS FOR LATTICE STRAINS

The stress state at the center of the compressed specimen in an opposed-anvil setup is given by,[12,14]

$$\sigma_{ij}=\begin{vmatrix}\sigma_{11}&0&0\\0&\sigma_{11}&0\\0&0&\sigma_{33}\end{vmatrix}$$
$$=\begin{vmatrix}\sigma_P&0&0\\0&\sigma_P&0\\0&0&\sigma_P\end{vmatrix}+\begin{vmatrix}-t/3&0&0\\0&-t/3&0\\0&0&2t/3\end{vmatrix}$$
$$=\sigma_P+D_{ij}, \tag{1}$$

where σ_{11} and σ_{33} are radial and axial stress components, respectively. σ_P is the mean normal stress (equivalent hydrostatic pressure). The uniaxial stress component $t=(\sigma_{33}-\sigma_{11})$ and D_{ij} is the deviatoric stress component. The strain produced by σ_P can become large at high pressures and is better analyzed using an appropriate equation of state. In terms of the measured d spacing, $d_m(hkl)$, the strain produced by D_{ij} is given by

$$\epsilon_D(hkl)=[d_m(hkl)-d_P(hkl)]/d_P(hkl), \tag{2}$$

where $d_P(hkl)$ is the spacing under the pressure σ_P alone. The equations for the lattice strains derived earlier[14–18] can be rearranged to give the following relation:

$$d_m(hkl)=d_P(hk)[1+(1-3\cos^2\psi)Q(hkl)], \tag{3}$$

where

$$Q(hkl)=(t/3)\{\alpha[2G_R^X(hkl)]^{-1}+(1-\alpha)(2G_V)^{-1}\}. \tag{4}$$

$G_R^X(hkl)$, termed x-ray shear modulus, is the aggregate shear modulus calculated under the Reuss (iso-stress) condition, the averaging being done only over the group of crystallites contributing to the diffracted intensity at the point of observation. G_V is the shear modulus under the Voigt (iso-strain) condition. The negative sign of t is included in Eq. (3) so that t is to be taken as a positive number in this article. The

0021-8979/98/83(12)/7567/9/$15.00

factor α, which lies between 0 and 1, decides in an actual case the relative weights of the strains calculated under Reuss and Voigt conditions.

The expressions for G_V in terms of S_{ij} for different crystal systems can be found elsewhere.[22] The expressions for $G_R^X(hkl)$ are as follows.

A. Cubic system

$$[2G_R^X(hkl)]^{-1}=[S_{11}-S_{12}-3(S_{11}-S_{12}-\tfrac{1}{2}S_{44})\Gamma(hkl)], \tag{5}$$

where

$$\Gamma(hkl)=(h^2k^2+k^2l^2+l^2h^2)/(h^2+k^2+l^2)^2.$$

B. Hexagonal system

$$[2G_R^X(hkl)_{\text{hex}}^{-1}=\tfrac{1}{2}[2S_{11}-S_{12}-S_{13})+l_3^2(-5S_{11}+S_{12}+5S_{13}-S_{33}+3S_{44})+l_3^4(3S_{11}-6S_{13}+3S_{33}-3S_{44})], \tag{6}$$

where $l_3^2=3a^2l^2/M^2$, $M^2=[4c^2(h^2+hk+l^2)+3a^2l^2]$, and a and c are the lattice parameters of the hexagonal cell. It is noted that l_3^2 is the same as B in Ref. 12.

C. Trigonal system

$$[2G_R^X(hkl)]^{-1}=[2G_R^X(hkl)]_{\text{hex}}^{-1}+3l_2l_3(3l_1^2-l_2^2)S_{14}+3l_1l_3(3l_2^2-l_1^2)S_{25}, \tag{7}$$

where $l_1=\sqrt{3}ch/M$, $l_2=c(h+2k)/M$, $l_3=\sqrt{3}al/M$. The expression of M is the same as for the hexagonal system. A hexagonal set of axes was used to define S_{ij}. For the trigonal classes 32, $\bar{3}m$, and $3m$, $S_{25}=0$.

D. Tetragonal system

$$[2G_R^X(hkl)]^{-1}=[2G_R^X(hkl)]_{\text{tetra}}^{-1}+\tfrac{3}{2}l_1^2l_2^2(-2S_{11}+2S_{12}+S_{66})+3l_1l_2(l_1^2-l_2^2)S_{16}, \tag{8}$$

where $l_1=ch/M$, $l_2=ck/M$, $l_3=al/M$, and $M^2=[a^2l^2+c^2(h^2+k^2)]$. $[2G_R^X(hkl)]_{\text{tetra}}^{-1}$ is obtained by using these values of l_3 and M in the expression for $[2G_R^X(hkl)]_{\text{hex}}^{-1}$. For classes $\bar{4}2m$, $4mm$, and 423, $S_{16}=0$.

E. Orthorhombic system

$$\begin{aligned}[2G_R^X(hkl)]^{-1}=\tfrac{1}{2}\{&-(S_{12}+S_{13}+S_{23})+l_1^2(S_{23}-S_{11})\\&+l_2^2(S_{13}-S_{22})+l_3^2(S_{12}-S_{33})\\&+3[l_1^4S_{11}+l_2^4S_{22}+l_3^4S_{33}\\&+l_1^2l_2^2(2S_{12}+S_{66})+l_2^2l_3^2(2S_{23}+S_{44})\\&+l_3^2l_1^2(2S_{13}+S_{55})]\},\end{aligned} \tag{9}$$

where, $l_1=hd(hkl)/a$, $l_2=kd(hkl)/b$, and $l_3=ld(hkl)/c$. $d(hkl)$ is the inter-planar spacing which can be expressed in terms of (hkl) and the unit cell dimensions, a, b and c, using the well known relation.

F. Monoclinic system

$$\begin{aligned}[2G_R^X(hkl)]^{-1}=\tfrac{1}{2}\{&S_{11}(3l_1^4-l_1^2)+S_{22}(3l_2^4-l_2^2)+S_{33}(3l_3^4-l_3^2)+S_{12}(6l_1^2l_2^2-l_1^2-l_2^2)+S_{13}(6l_1^2l_3^2-l_1^2-l_3^2)\\&+S_{23}(6l_2^2l_3^2-l_2^2-l_3^2)+l_1l_3[S_{15}(6l_1^2-1)+S_{25}(6l_2^2-1)+S_{35}(6l_3^2-1)]+6S_{46}l_1l_2^2l_3\\&+3(S_{44}l_2^2l_3^2+S_{55}l_3^2l_1^2+S_{66}l_1^2l_2^2)\},\end{aligned} \tag{10}$$

where, $l_1=hd(hkl)/a$, $l_2=kd(hkl)/b$ and with monoclinic angle, β, $l_3=(al-hc\cos\beta)d(hkl)/ac\sin\beta$.

G. Triclinic system

$$\begin{aligned}[2G_R^X(hkl)]^{-1}=\tfrac{1}{2}[&S_{11}(3l_1^4-l_1^2)+S_{22}(3l_2^4-l_2^2)+S_{33}(3l_3^4-l_3^2)+S_{12}(6l_1^2l_2^2-l_1^2-l_2^2)+S_{13}(6l_1^2l_3^2-l_1^2-l_3^2)\\&+S_{23}(6l_2^2l_3^2-l_2^2-l_3^2)+(6l_1^2-1)(S_{14}l_2l_3+S_{15}l_3l_1+S_{16}l_1l_2)+(6l_2^2-1)(S_{24}l_2l_3+S_{25}l_3l_1+S_{26}l_1l_2)\\&+(6l_3^2-1)(S_{34}l_2l_3+S_{35}l_3l_1+S_{36}l_1l_2)+6l_1l_2l_3(S_{56}l_1+S_{46}l_2+S_{45}l_3)+3(S_{44}l_2^2l_3^2+S_{55}l_3^2l_1^2+S_{66}l_1^2l_2^2)],\end{aligned} \tag{11}$$

where, $l_1=(hb-ak\cos\gamma)d(hkl)/ab\sin\gamma$, $l_2=kd(hkl)/b$, and $l_3=(Y/Z)d(hkl)$. Y and Z are given by

$$Y=abl\sin^2\gamma+bch(\cos\alpha\cos\gamma-\cos\beta)+ack(\cos\beta\cos\gamma-\cos\alpha),$$

and

$$Z=abc(1-\cos^2\alpha-\cos^2\beta-\cos^2\gamma+2\cos\alpha\cos\beta\cos\gamma)^{1/2}\sin\gamma.$$

For choice of axes in monoclinic and triclinic systems, see Ref. 23. It should be noted that the unit cell parameters and the S_{ij} terms appearing in these equations are at pressure σ_P.

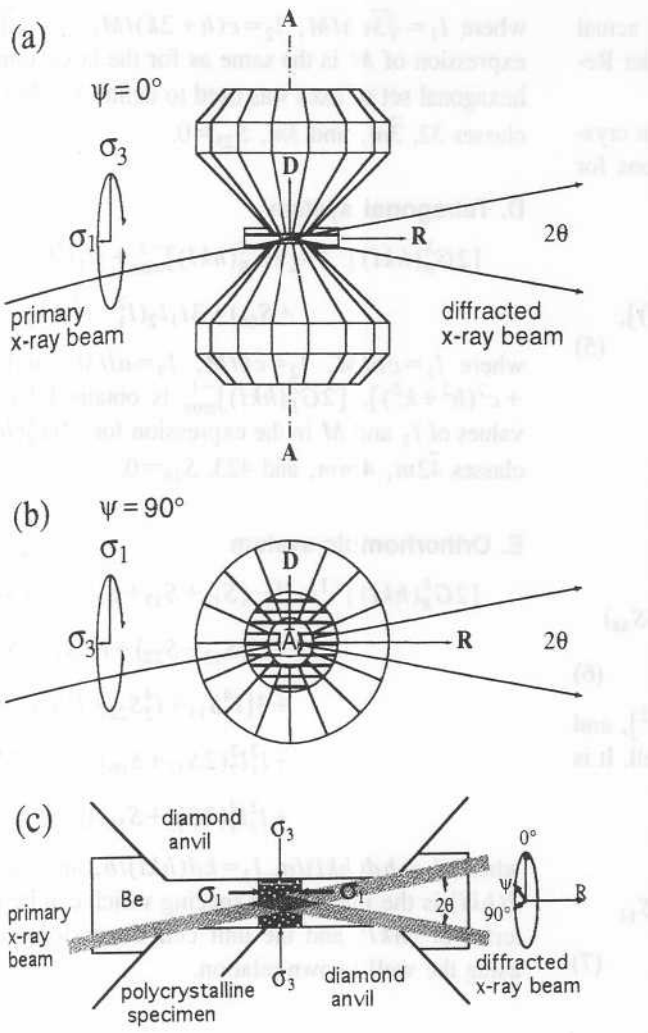

FIG. 1. The diffraction geometry for measuring d spacings as a function of angle ψ.

III. EXPERIMENTAL SETUP

A detailed analysis of the diffraction data under NSS becomes possible if the d spacings are measured for different ψ angles. This was achieved by modifying[20,21] the radial geometry,[24] which suffered from the disadvantage that the primary x-ray beam passed through the entire sample having a pressure differential ranging from 1 bar to the peak pressure. In the present experiments the effects of radial stress gradients were minimized by using samples (typically a disk of 10 μm thickness and 25 μm diameter) which were small in comparison with the diamond culet (e.g., 400 μm diameter). The sample is confined at the center of the anvil face with the help of a high-strength Be gasket which is transparent to high energy x rays (Fig. 1). The magnitude of the uniaxial stress component in the sample is deliberately enhanced by not using a pressure-transmitting medium. A fine primary x-ray beam (down to 5 μm) from the synchrotron source[25] is used and the diffraction data are recorded using the energy dispersive mode. With a double-collimator system, only a signal from the sample at the interception of primary and diffracted beams is received by the detector and the signal from the Be gasket is supressed.[20,21,26] With this arrangement, the radial variation of the lattice strain (stress gradient) is found to be negligible in comparison with the directional variation arising from the uniaxial stress component. The diamond cell was rotated about an axis (R, Fig. 1) perpendicular to the load axis and bisecting the 2θ diffraction angle. The diffraction patterns for the reflections in the 20–60 keV range were collected at 10° increment of ψ. The analysis of the data on fcc-$Fe_{0.94}O$ (simply referred to as FeO), bcc-Fe, and hcp-Fe is discussed in this article.

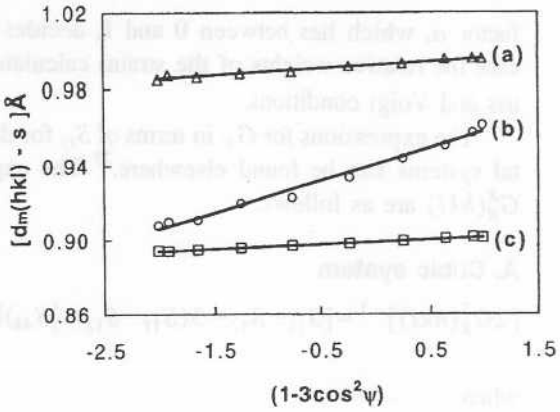

FIG. 2. $d_m(hkl)$ vs $(1-3\cos^2\psi)$ plots: (a) (201) for ϵ-Fe at 52 GPa, $s=0$. (b) (111) for FeO at 8.3 GPa, $s=1.5$ Å. (c) (310) for α-Fe at 4.6 GPa, $s=0$. Errors in $d_m(hkl)$ for (a) and (c) are less than the size of the symbols, and nearly of the size of the symbols for (b).

IV. ANALYSIS OF THE DATA

A. General

The ψ dependence of the measured d spacings given by Eq. (3) is general and valid for all crystal systems. Typical $d_m(hkl)$ vs $(1-3\cos^2\psi)$ plots are shown in Fig. 2. It is seen that Eq. (3) fits these data very well. Similar fits were obtained for nearly 50 data sets (cubic FeO to 12 GPa, α-Fe to 14 GPa, and ϵ-Fe to 200 GPa). The R^2 values ranged from 0.99 in the lower pressure region to 0.95 in the 200 GPa range.

1. Strain due to σ_P

The intercept of the $d_m(hkl)$ vs $(1-3\cos^2\psi)$ plot (Fig. 2) gives $d_P(hkl)$, the d spacing corresponding to the hydrostatic stress component σ_P. The lattice parameters a_P and c_P, calculated from $d_P(hkl)$ values, correspond to the values under hydrostatic compression. The lattice parameters for cubic and rhombohedral FeO, α-Fe, and ϵ-Fe, calculated from the $d_P(hkl)$ values are listed in Table I. The data obtained with the conventional diamond cell geometry, using

TABLE I. Effect of nonhydrostatic compression on the lattice parameter (Å).

P (GPa)	FeO (fcc) 8.3	FeO (rhomb.) 19	α-Fe (bcc) 4.6	ϵ-Fe (hcp) 52
a_P	4.230 (2)	2.887 (3)	2.8417 (9)	2.3736 (7)
a_ψ	4.252 (11)	2.891 (10)	2.8482 (15)	2.381 (6)
c_P	...	7.344 (10)	...	3.7896 (3)
c_ψ	...	7.428 (60)	...	3.795 (2)
V_P	75.67 (6)	53.01 (13)	22.948 (12)	36.98 (2)
V_ψ	76.85 (34)	53.77 (57)	23.105 (20)	37.25 (18)

energy dispersive mode, correspond approximately to the data at $\psi=85°$. For comparison, the lattice parameters, a_ψ and c_ψ, calculated with $d_m(hkl)$ at $\psi=85°$ are also listed in Table I. These values correspond to the lattice parameters obtained if the data are collected using the conventional diamond cell diffraction geometry and the effect of NSS on the lattice strains is ignored. It is seen that the standard deviations in a_P and c_P are much smaller than those in a_ψ and c_ψ. Many more data sets showed a similar trend; the standard deviations in a_ψ and c_ψ were 2–10 times larger than the corresponding values for a_P and c_P. The unit cell volumes calculated from a_P and c_P are significantly smaller than the corresponding volumes calculated from a_ψ and c_ψ. This suggests that the volume strain is underestimated if the effect of NSS is ignored, an effect observed experimentally quite early[10] and explained quantitatively later.[27]

2. Estimation of t

The estimation of t has attracted considerable attention in the past since it offers an elegant and the only method of estimating as a function of pressure the maximum shear stress[12,14,28] supported by the specimen material. A group of investigators[28–31] used isotropic elasticity theory while many others[19,32–36] used lattice-strain equations to analyze the diffraction data. A discussion of the earlier work, including the estimation of t by the measurement of pressure gradient, can be found in a recent publication.[34] The estimation of t using lattice-strain equations requires the knowledge of the single crystal elastic moduli at σ_P, which can be obtained by extrapolating to high pressures the ultrasonic elasticity data measured at low pressure. The following relation for the cubic system, which can be derived from Eqs. (4) using the approach outlined earlier,[35] has definite advantage over the forms of equations used earlier:

$$\begin{aligned} &t=(6G)\langle Q(hkl)\rangle f(x),\\ &f(x)=A/B,\\ &A=\{[(2x+3)/10]+5x/2(3x+2)\},\\ &B=\{\alpha[x-3(x-1)\langle\Gamma(hkl)\rangle]+5x(1-\alpha)/(3x+2)\}, \end{aligned} \tag{12}$$

where the angle brackets denote the average for all the observed reflections, $x=2(S_{11}-S_{12})/S_{44}$ denotes the elastic anisotropy, and G is the aggregate shear modulus of the specimen material at σ_P. For an isotropic case ($x=1$), $f(x)=1$. Even for moderately large anisotropy $f(x)\cong 1$. For example, for $\alpha=1$, $f(x)$ increases monotonically from 0.80 at $x=3$ to 1 at $x=1$, and then decreases with a decrease in x, and reaches 0.85 at $x=0.2$. For $\alpha=0.5$, the $f(x)$ values are 0.96 and 1.05, respectively, for $x=3$ and $x=0.2$. As discussed in Sec. IV B, x can be determined from $Q(hkl)$ values without requiring the value of t, and therefore $f(x)$ can be calculated in cases of a high degree of elastic anisotropy for which $f(x)$ deviates from unity significantly.

The determination of the averages of $Q(hkl)$ and $\Gamma(hkl)$ requires that the reflections be in the complete range of $\Gamma(hkl)$ (i.e., 0–1). Often, the full range of reflections are not recorded in the high pressure experiments. In such cases, $Q(hkl)$ for missing reflections can be estimated from the $Q(hkl)-\Gamma(hkl)$ plots, and used for evaluating the averages. For lower symmetry crystal systems, more than one parameter (e.g., three for hexagonal) is required to define elastic anisotropy. The functional form of $f(x)$ changes, but it remains close to unity.

TABLE II. Uniaxial stress components for fcc FeO, α-Fe, and ϵ-Fe with $\alpha=1$.

	FeO (fcc)	α-Fe (bcc)	ϵ-Fe (hcp)
P (GPa)	8.3	4.6	52
G (GPa)	45.6[a]	90[b]	175[b]
t (GPa)	1.4 (2)[c]	1.2 (1)	4.4 (2)
t/G	0.03	0.01	0.02

[a]Extrapolation (second degree polynomial in pressure) of ultrasonic data (Ref. 34).
[b]Extrapolation (linear in pressure) of ultrasonic data (Ref. 35).
[c]Choice of $\alpha=0.5$ increases t by 14%, 8%, and 5%, respectively, for FeO, α-Fe, and ϵ-Fe. The increase in t values is nearly equal to the errors of measurement.

The use of Eq. (12) in estimating t has the advantage over the other ways[19,32,33] of using the lattice-strain equations in that it requires only the extrapolation of G (as opposed to single crystal elastic elastic moduli) to high pressures. An extrapolation linear in pressure is adequate at low volume compressions, while the equations based on finite strain theory[37,38] can be used for large compressions. Equation (12) with $f(x)=1$ has been used recently[34] in analyzing the data on iron and tungsten to 300 GPa.

The estimation of t of a pressure-induced phase poses some difficulty, as G_0 and G_0' of the high-pressure phase are often not known. The extrapolation of the data on the one-atmosphere phase does not predict precisely G for the high-pressure phase, as G is expected to change across the transition. Two sources contribute to this change. The volume decrease associated with a pressure-induced transition causes G to increase. The use of a finite strain equation for the extrapolation of the data fully accounts for this change only if G_0' does not change across the transition. The second source is the structural change during the transition. It is difficult to estimate the contribution from this source. The t values for both $\alpha=1$ and $\alpha=0.5$ for FeO (8.3 GPa, α-Fe (4.6 GPa), and ϵ-Fe (52 GPa) are listed in Table II. The maximum shear stress levels (equal to the uniaxial stress components) in all three cases are much smaller than the values obtained from the predicted relation for the theoretical[39] yield stress ($\approx 0.2G$).

The uniaxial stress component in the sample has been measured recently[40] by placing a layer of gold calibrant on top of the sample. In this configuration, the axial stress components in the sample and calibrant are equal (required by the codition of stress continuity at the sample–calibrant interface), while the radial stress components are different. The $d_m(hkl)$ vs ψ data on both the sample and calibrant, and the knowledge of the shear modulus of the calibrant, are used to obtain t in the sample. The results of these measurements agree very well with those obtained from Eq. (12).

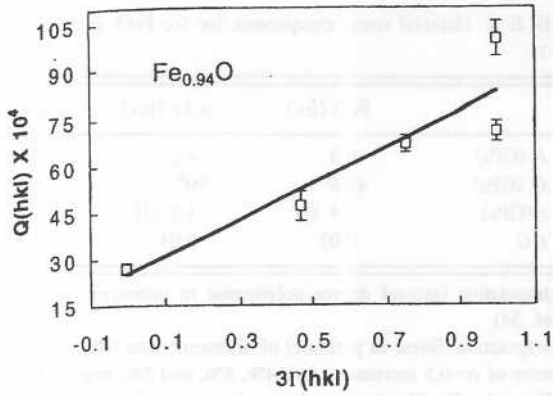

FIG. 3. $Q(hkl)$ vs $3\Gamma(hkl)$ plot for FeO at 8.3 GPa. The slope and intercept are $m_1=0.0058(10)$ and $m_0=0.0025(7)$, respectively.

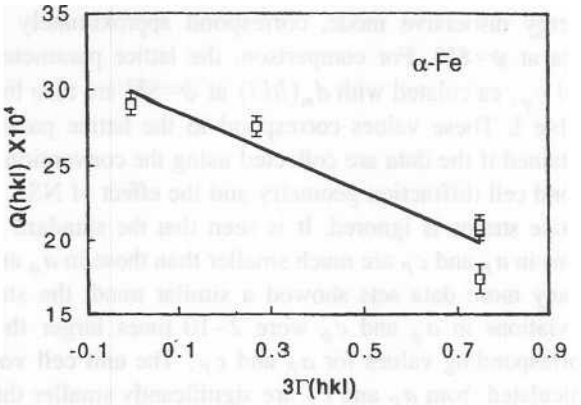

FIG. 4. $Q(hkl)$ vs $3\Gamma(hkl)$ plot for α-Fe at 4.6 GPa. The slope and intercept are $m_1=-0.00134(30)$ and $m_0=0.00299(20)$, respectively.

B. Analysis of $Q(hkl)$

An attempt[41] was made earlier to extract the information on S_{ij} by analyzing the data on NaCl under NSS. The diffraction patterns were recorded on a film using conventional diamond cell geometry. Only limited information could be obtained because reflections with only slightly differing ψ angles could be recorded. The $Q(hkl)$ values obtained from the $d_m(hkl)$ vs $(1-3\cos^2\psi)$ plots contain information on S_{ij}. A method of estimating S_{ij} by analyzing $Q(hkl)$ has been suggested recently.[42] The details of the method are discussed in this section.

1. Cubic system

Determination of elastic anisotropy: Equations (4) and (5) suggest that $Q(hkl)$ vs $\Gamma(hkl)$ plot is a straight line, with the intercept, m_0, and slope, m_1, given by

$$m_0=(\alpha t/3)\left[(S_{11}-S_{12})+\frac{5}{2}(\alpha^{-1}-1)\frac{(S_{11}-S_{12})S_{44}}{3(S_{11}-S_{12})+S_{44}}\right], \tag{13a}$$

$$m_1=-(\alpha t/3)(S_{11}-S_{12}-S_{44}/2), \tag{13b}$$

$$(m_0/m_1)=-[x/(x-1)][1+5(\alpha^{-1}-1)/(3x+2)]. \tag{13c}$$

The $Q(hkl)$ vs $\Gamma(hkl)$ plots are shown in Figs. 3 and 4 for FeO and α-Fe, respectively. The elastic anisotropy, x, can be determined from Eq. (13c) which does not involve t. However, x obtained from Eq. (13c) is sensitive to the choice of α. For a given value of (m_0/m_1), the inferred elastic anisotropy is lowest with $\alpha=1$, and increases with decreasing α. The x value can be used to compute $f(x)$, which is required to obtain t from Eq. (12). It is easily verified that although x is sensitive to the choice of α, $f(x)$ varies within only $\approx$15% for any consistent set of α and x in the range $1\geq\alpha\geq0.5$ and $3\geq x\geq0.2$. The x values for FeO and α-Fe for both $\alpha=1$ and $\alpha=0.5$ are listed in Table III.

Estimation of S_{ij}: Of the three equations needed to obtain all S_{ij} terms, two are provided by Eqs. (13a) and (13b). The third relation is derived from the bulk modulus, K, at σ_P,

$$S_{11}+2S_{12}=1/(3K), \tag{13d}$$

where K can be obtained at any desired pressure using a standard equation of state. The S_{ij} for FeO and α-Fe were

TABLE III. The elastic moduli of FeO, α-Fe, and ϵ-Fe at high pressure. The standard errors (in parenthesis) were derived the errors in $Q(hkl)$; moduli units in GPa.

	FeO 8.3 GPa			α-Fe 4.6 GPa			ϵ-Fe 52 GPa		
	$\alpha=0.5$	$\alpha=1$	Ultras.[a]	$\alpha=0.5$	$\alpha=1$	Ultras.[b]	$\alpha=0.5$	$\alpha=1$	Theory[c]
C_{11}	413 (73)	313 (44)	283 (5)	260 (17)	281 (18)	262 (5)	552 (65)	639 (55)	638
C_{12}	77 (37)	123 (22)	144 (2)	154 (14)	144 (12)	155 (2)	335 (60)	300 (55)	190
C_{13}	...	...	...	...	...	...	301 (45)	254 (41)	218
C_{33}	...	...	...	...	...	...	562 (80)	648 (83)	606
C_{44}	20 (4)	28 (7)	36 (1)	153 (40)	123 (30)	128 (2)	395 (30)	422 (23)	178
C'[d]	168 (41)	93 (25)	78 (13)	53 (11)	68 (11)	53 (3)	...	...	...
x	0.12 (3)	0.3 (1)	0.52 (2)	2.9 (8)	1.8 (6)	2.4 (1)	3.6 (1.5)[e]	2.5 (6)[e]	0.79[e]

[a] Extrapolation of ultrasonic data to 3 GPa in Ref. 44.
[b] Extrapolation of ultrasonic data to 1 GPa in Ref. 45.
[c] Results from Ref. 48 calculated at $V=9.70$ Å^3/atom, which is close to the experimental volume at 52 GPa ($V=9.93$ Å^3/atom, Ref. 43); similar results were obtained in Ref. 49.
[d] $C'=(C_{11}-C_{12})/2$.
[e] C_{44}/C_{66}, $C_{66}=(C_{11}-C_{12})/2$.

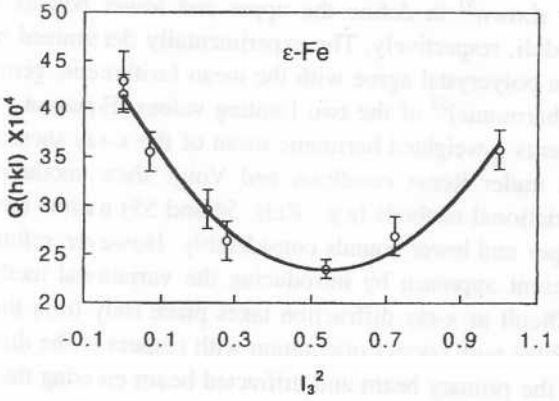

FIG. 5. $Q(hkl)$ vs l_3^2 plot for ϵ-Fe at 52 GPa. A parabolic fit [Eq. (14a)] gives $m_0=4.13(1)\times10^{-3}$, $m_1=-6.63(5)\times10^{-3}$, and $m_2=6.15(7)\times10^{-3}$.

calculated for $\alpha=1$ and 0.5, and the resulting C_{ij} are listed in Table III. For comparison, the C_{ij} values obtained by the extrapolation (linear in pressure) of the one-atmosphere elastic constants using their pressure derivatives are also listed.

2. Hexagonal system

Equations (4) and (6) can be combined to give the following relation:

$$Q(hkl)=m_0+m_1l_3^2+m_2l_3^4, \tag{14a}$$

where

$$m_0=(\alpha t/6)[2S_{11}-S_{12}-S_{13}+(\alpha^{-1}-1)(2G_V)^{-1}], \tag{14b}$$

$$m_1=(\alpha t/6)[-5S_{11}+S_{12}+5S_{13}-S_{33}+3S_{44}] \tag{14c}$$

$$m_2=(\alpha t/6)[3S_{11}-6S_{13}+3S_{33}-3S_{44}] \tag{14d}$$

The axial compressibilities provide two more relations:

$$\chi_a=\alpha(S_{11}+S_{12}+S_{13})+(1-\alpha)(3K_V)^{-1} \tag{14e}$$

$$\chi_c=\alpha(S_{33}+2S_{13})+(1-\alpha)(3K_V)^{-1}. \tag{14f}$$

The $Q(hkl)$ vs l_3^2 plot (Fig. 5) for ϵ-Fe at 52 GPa indicates that the data fit Eq. (14a) very well. The axial compressibilities at 52 GPa were derived from the measured[43] volume compressibility and the pressure dependence of the axial ratio (c/a) using the following relations:

$$2\chi_a+\chi_c=\chi_{\rm vol}, \tag{14g}$$

$$\chi_a-\chi_c=[d(c/a)/dP]/(c/a). \tag{14h}$$

The S_{ij} were calculated first with $\alpha=1$. G_V calculated with these values was used to obtain the first set of S_{ij} with $\alpha=0.5$. Three iterations were needed to get a set of S_{ij} which did not change significantly on further iteration. The resulting C_{ij} for both $\alpha=1$ and $\alpha=0.5$ are listed in Table III.

The C_{ij} derived with $\alpha=1$ for FeO agrees within the errors of measurement with the corresponding values obtain from the extrapolation of the ultrasonic data.[44] With $\alpha=0.5$, C_{ij} show larger deviations from the extrapolated ultrasonic data although the differences are still within the combined uncertainties in the present estimates and extrapolated values. The softening of C_{44} under pressure seen in the present study is in agreement with the ultrasonic measurements up to 3 GPa. The lowest inferred elastic anisotropy is larger than the extrapolated value. It is likely that the pressure dependence of C_{44} is nonlinear in pressure, exhibiting a steeper decrease than predicted by a linear dependence. The results for α-Fe for both $\alpha=1$ and 0.5 agree well with the extrapolated ultrasonic data,[45] the agreement in the latter case being better. The results do not suggest softening of C_{44} as found in some bcc-structured materials.[46] It has been predicted that at higher pressures the modulus $C'=(C_{11}-C_{12})/2$ should soften and vanish above a critical pressure; i.e., the reentrant bcc phase proposed at higher pressures should become unstable with respect to a tetragonal distortion.[47,48] The measured C' in fact increases with pressure.

For ϵ-Fe, C_{11}, C_{33}, and C_{13} obtained from the present analysis with both $\alpha=1$ and 0.5 agree (within errors of measurement) with the GGA calculations,[48] but C_{12} and C_{44} differ markedly. The analysis with $\alpha=1$ gives the lowest estimate of C_{44}/C_{66} (a value of 2.5), which deviates significantly from the condition $C_{44}\cong C_{66}$ satisfied by most hcp metals. Since t for ϵ-Fe has been estimated, ignoring a possible increase in shear modulus across the $\alpha\rightarrow\epsilon$ transition, we looked for the probable cause of this discrepancy in the incorrect choice of t. However, calculations of C_{ij} with different t values indicate that C_{44}/C_{66} is extremely insensitive to the value of t; a fivefold increase in t results in an increase in C_{44}/C_{66} by only 8%. The relatively large value of C_{44}/C_{66} requires further scrutiny as it has important implications in the interpretation of reported anisotropy of the earth's inner core.[40,49]

V. DISCUSSION

It is seen from Eqs. (2) and (3) that the strain produced by the deviatoric stress component vanishes if the measurements are made at $\psi=\cos^{-1}(1/\sqrt{3})$, and $d_P(hkl)$ is directly measured. However, as discussed earlier, the effect of error in setting the ψ angle on $d_P(hkl)$ is maximum at this ψ value. The determination of $Q(hkl)$ and the parameters (t and S_{ij}) derived thereof, requires that $d_m(hkl)$ be at minimum of two ψ values. The measurements at $\psi=0°$ and 90° are preferred to any other set of ψ values, as these represent two extreme points on the $d_m(hkl)$ vs $(1-3\cos^2\psi)$ plot. Further, for a given error in setting the ψ angle, the errors in $d_P(hkl)$ and $Q(hkl)$ are minimum for these settings. Such measurements have been made with a modified Drickamer cell.[19] This setup,[19] however, has a limited high-pressure capability. The measurements at a number of ψ values are preferred over those at two settings, as the data are amenable to an easier statistical analysis.

The standard errors in $Q(hkl)$ shown in Figs. 3–5 were derived from the scatters in the $d_m(hkl)$ vs $(1-3\cos^2\psi)$ plots. These scatters represent the combined effects of the intrinsic error in the measurements $d_m(hkl)$, uncertainty in the ψ settings, and the shift of the probed region of the sample when the ψ angle is changed. The error in the mea-

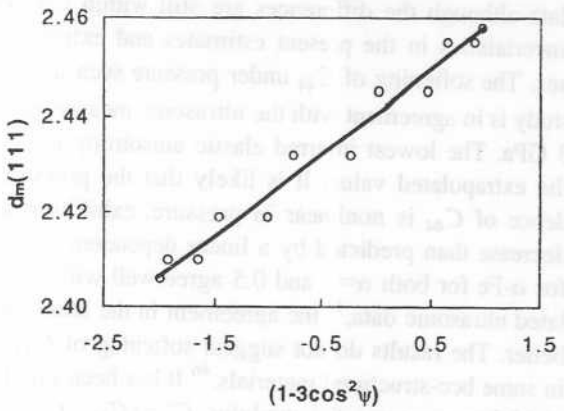

FIG. 6. Effect of error in ψ setting on $d_m(hkl)$ vs $(1-3\cos^2\psi)$ plot for (111) reflection of FeO.

surement of d spacings, based only on the precision in locating the diffraction-peak position, is ≈ 1 in 10^4. While the incremental steps in ψ can be set with a precision of $1'$ are, setting $\psi=0$ can be done at best with a certainty of $\pm 5°$. This results in a constant offset in all the ψ settings. The calculated effect of a 5° error in setting $\psi=0$ is shown in Fig. 6 for the (111) reflection of FeO at 8.3 GPa. The solid line represents the data with the correct setting. The open circles above the solid line represent the data in case the experimentally set ψ values are uniformly 5° more than the corresponding correct values. A straight line fit to these data suggests that the slope and intercept are overestimated by 0.5% and 0.1%, respectively. In case the set ψ values are 5° less than the corresponding correct values (lower open circles), the slope is overestimated (0.5%) and the intercept underestimated (0.1%). In both cases the scatter in the data increases marginally ($R^2=0.992$).

The best possible alignment procedure sets the ψ axis at the geometric center of the specimen (also the center of the volume enclosed by the interception of the primary and diffracted beams) with an uncertainty of ± 5 μm. Because of this small offset, the sample region probed by x rays shifts with the change in ψ setting. The $d_m(hkl)$ values at different ψ settings represent measurements at different sample regions of varying average pressure. For a given offset, the severity of the effect on $d_m(hkl)$ vs $(1-3\cos^2\psi)$ plot depends on the magnitude of the radial pressure gradient (which is expected to become appreciable at very high pressures), and the relative position of the ψ axis with respect to the sample region probed. For example, if on changing ψ from 0° to 90°, the probed region shifts gradually from a region of lower pressure (average) to a higher pressure region and back to a lower pressure region, then the data will fall on a C-shaped curve (concave upward). In general, this effect will manifest as a nonlinearity in the $d_m(hkl)$ vs $(1-3\cos^2\psi)$ plots. This effect is not noticeable in the data analyzed presently, probably because of small radial pressure gradients.

The stress state in the crystallites constituting a polycrystal is complex. The elastic moduli of a polycrystal in terms of the single crystal moduli have been derived under the assumptions of strain (Voigt)[50] and stress (Reuss)[51] continuities across the boundaries separating the crystallites, which are shown[52] to define the upper and lower bounds of the moduli, respectively. The experimentally determined moduli of a polycrystal agree with the mean (arithmetic, geometric, or harmonic)[51] of the two limiting values. Equation (4) represents a weighted harmonic mean of the x-ray shear modulus under Reuss condition and Voigt shear modulus. The variational methods (e.g., Refs. 54 and 55) narrow down the upper and lower bounds considerably. *However,* refining the present approach by introducing the variational methods is difficult as x-ray diffraction takes place only from the crystallites with correct orientation with respect to the directions of the primary beam and diffracted beam entering the detector.

The specimen compressed in an opposed-anvil setup undergoes considerable plastic flow before the equilibrium stress condition is established. The magnitude of the deviatoric stress component depends on the plastic flow of the specimen. A large deviatoric stress component can cause yielding of the crystallites, and the stress state in such a case is closer to the Reuss condition. A small magnitude of this component will produce elastic strain resulting in a stress state closer to Voigt condition. For these reasons, *a priori* choice of a in an actual experiment is difficult. The analysis[19] of high pressure x-ray diffraction data on NaCl suggests that a= I in the low pressure region, and tends to approach a=Q.5 as the pressure is increased. However, this trend is characteristic of the deformation behavior of the specimen in the high-pressure setup (a modified Drickamer cell) used in the experimen,[19] and cannot be generalized. It should be noted that the determination of dp(hkl) from the d_{ψ}(h *k*l) *vs (1 - 3 cost* $^{O)}$ plots does not depend on the choice of *a.* Among the other *parameters. i* is least and x is most sensitive to the choice of a. The changes brought about in the estimated C_{ij} on changing a from I to 0.5 stay within the errors of measurement: the changes are such that it produces a large effect on x. In this respect these changes are systematic.

In the high-pressure environment, the yielding of the crystallites under the action of a deviatoric stress component is complex. The equations in this article are derived assuming a single t value for the crystallites of different orientations with respect to the load axis. The yielding of a single crystal at atmospheric pressure is strongly orientation-dependent, and it may appear logical to consider an hkl-dependent t. A simple analysis of the scatter in the data suggests that the equations with a constant t are consistent with the experimental observations. The errors in $Q(hkl)$ are derived from the scatter in the $d_m(hkl)$ versus $(1-3\cos^2\psi)$ plot for each reflection and combined to give an overall uncertainty, Δ_1, $Q(hkl)$, Δ_1 being 0.0007 (3), 0.0001 (0), and 0.0002 (1) for FeO, α-Fe, and ϵ-Fe, respectively. The numbers in parentheses are the standard deviations. Equation (3) on which these plots are based is also valid for each reflection with different t values. The assumption of a constant t enters only in Eqs. (13a) and (14a), which predict, respectively, a linear $Q(hkl)$ vs $\Gamma(hkl)$ and a parabolic $Q(hkl)$ vs l_3^2 plot. The errors (Δ_2) in $Q(hkl)$, derived from these plots are 0.001, 0.0002, and 0.0001 for FeO, α-Fe, and ϵ-Fe, respectively. A possible violation of the as-

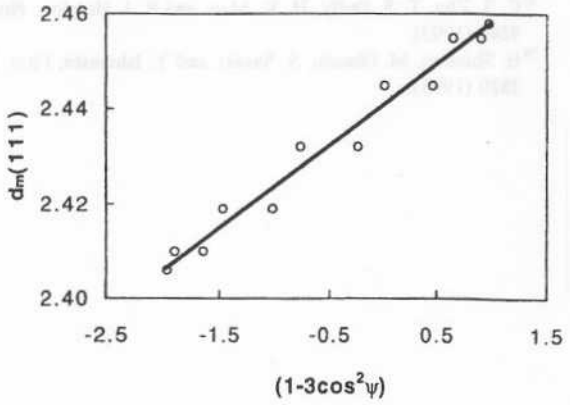

FIG. 6. Effect of error in ψ setting on $d_m(hkl)$ vs $(1-3\cos^2\psi)$ plot for (111) reflection of FeO.

surement of d spacings, based only on the precision in locating the diffraction-peak position, is ≈ 1 in 10^4. While the incremental steps in ψ can be set with a precision of $1'$ are, setting $\psi=0$ can be done at best with a certainty of $\pm 5°$. This results in a constant offset in all the ψ settings. The calculated effect of a 5° error in setting $\psi=0$ is shown in Fig. 6 for the (111) reflection of FeO at 8.3 GPa. The solid line represents the data with the correct setting. The open circles above the solid line represent the data in case the experimentally set ψ values are uniformly 5° more than the corresponding correct values. A straight line fit to these data suggests that the slope and intercept are overestimated by 0.5% and 0.1%, respectively. In case the set ψ values are 5° less than the corresponding correct values (lower open circles), the slope is overestimated (0.5%) and the intercept underestimated (0.1%). In both cases the scatter in the data increases marginally ($R^2=0.992$).

The best possible alignment procedure sets the ψ axis at the geometric center of the specimen (also the center of the volume enclosed by the interception of the primary and diffracted beams) with an uncertainty of ± 5 μm. Because of this small offset, the sample region probed by x rays shifts with the change in ψ setting. The $d_m(hkl)$ values at different ψ settings represent measurements at different sample regions of varying average pressure. For a given offset, the severity of the effect on $d_m(hkl)$ vs $(1-3\cos^2\psi)$ plot depends on the magnitude of the radial pressure gradient (which is expected to become appreciable at very high pressures), and the relative position of the ψ axis with respect to the sample region probed. For example, if on changing ψ from 0° to 90°, the probed region shifts gradually from a region of lower pressure (average) to a higher pressure region and back to a lower pressure region, then the data will fall on a C-shaped curve (concave upward). In general, this effect will manifest as a nonlinearity in the $d_m(hkl)$ vs $(1-3\cos^2\psi)$ plots. This effect is not noticeable in the data analyzed presently, probably because of small radial pressure gradients.

The stress state in the crystallites constituting a polycrystal is complex. The elastic moduli of a polycrystal in terms of the single crystal moduli have been derived under the assumptions of strain (Voigt)[50] and stress (Reuss)[51] continuities across the boundaries separating the crystallites, which are shown[52] to define the upper and lower bounds of the moduli, respectively. The experimentally determined moduli of a polycrystal agree with the mean (arithmetic, geometric, or harmonic)[53] of the two limiting values. Equation (4) represents a weighted harmonic mean of the x-ray shear modules under Reuss condition and Voigt shear modulus. The variational methods (e.g.. Refs. 54 and 55) narrow down the upper and lower bounds considerably. However, refining the present approach by introducing the variational methods is difficult as x-ray diffraction takes place only from the crystallites with correct orientation with respect to the directions of the primary beam and diffracted beam entering the detector.

The specimen compressed in an opposed-anvil setup undergoes considerable plastic flow before the equilibrium stress condition is established. The magnitude of the deviatoric stress component depends on the plastic flow of the specimen. A large deviatoric stress component can cause yielding of the crystallites, and the stress state in such a case is closer to the Reuss condition. A small magnitude of this component will produce elastic strain resulting in a stress state closer to Voigt condition. For these reasons, *a priori* choice of a in an actual experiment is difficult. The analysis[19] of high pressure x-ray diffraction data on NaCI suggests that a=1 in the low pressure region, and tends to approach a=0.5 as the pressure is increased. However, this trend is characteristic of the deformation behavior of the specimen in the high-pressure setup (a modified Drickamer cell) used in the experimen, [19] and cannot be generalized. It should be noted that the determination of $d_n(hkl)$ from the $d_{,,}(hk1)$ vs $(1-3\cos^t \psi)$ plots does not depend on the choice of a. Among the other parameters, t is least and x is most sensitive to the choice of a. The changes brought about in the estimated $C_{,1}$ on changing a from I to 0.5 stay within the errors of measurement; the changes are such that it produces a large effect on x. In this respect these changes are systematic.

In the high-pressure environment, the yielding of the crystallites under the action of a deviatoric stress component is complex. The equations in this article are derived assuming a single t value for the crystallites of different orientations with respect to the load axis. The yielding of a single crystal at atmospheric pressure is strongly orientation-dependent. and it may appear logical to consider an hkl-dependent t. A simple analysis of the scatter in the data suggests that the equations with a constant t are consistent with the experimental observations. The errors in Q(hkl) are derived from the scatter in the $d_{,,}(hk1)$ versus $(1-3\cos^t \psi)$ plot for each reflection and combined to give an overall uncertainty, A_{1}. Q(hkl), $_{1}$ being 0.0007 (3), 0.0001 (0). and 0.0002 (1) for FeO. a-Fe, and e-Fe, respectively. The numbers in parentheses are the standard deviations. Equation (3) on which these plots are based is also valid for each reflection with different t values. The assumption of a constant i enters only in Eqs. (13a) and (14a), which predict, respectively, a linear Q(hkl) vs 1_(hkl) and a parabolic $Q(hkl)$ vs 1 plot. The errors ($A_{,}$) in $Q(hkl)$. thrived from these plots are 0.001. 0.0002, and 0.0001 for FeO. a-Fe. and c-Fe. respectively. A possible violation of the as-

s4B yroener, Z. Phys. **151,** 504 (1958).
5[5] 2. Hashin and 5. Sh[riknlan. J. Mcch- Phys- Solids 10. 335 (1962): 10, 343 (1962)-
wA. K. Singh and C. Balasingh (unpublished).
[57] C. S. Zha, T. 5. Duffy, H. K- Mao, and R. J- Hemlcy. Phys- Rev. B 48, 9246 (1993),
[58] H. Shimizu, M- Ohnishi, S. 5asaki, and Y. Ishibashi. Plays. Rev. Lett. 74, 2820 (1995)-